Journal of Molecular Graphics and Modelling 30 (2011) 54–66

Contents lists available at ScienceDirect

Journal of Molecular Graphics and Modelling

journal homepage: www.elsevier.com/locate/JMGM

QM and QM/MD simulations of the Vinca alkaloids docked to tubulin

Evan B. Kelly[a,1], Jack A. Tuszynski[b,*], M. Klobukowski[a]

[a] Department of Chemistry, University of Alberta, Edmonton, Alberta T6G 2G2, Canada
[b] Division of Experimental Oncology, Cross Cancer Institute, Edmonton, Alberta T6G 1Z2, Canada

ARTICLE INFO

Article history:
Received 8 April 2011
Received in revised form 3 June 2011
Accepted 8 June 2011
Available online 2 July 2011

Keywords:
QM/MD simulations
Vinca alkaloids
Vinblastine
Vincristine
Vindesine
Vinorelbine
Vinflunine

ABSTRACT

The *Vinca* alkaloids are a class of pharmaceutically relevant binary indole-indoline alkaloids based on and including natural extracts of the periwinkle plant, *Catharanthus rosea*. Two natural products, vinblastine and vincristine, have been in clinical use as important chemotherapy agents for over four decades. Two semi-synthetic *Vinca* alkaloids, vindesine and vinorelbine, are currently in investigational chemotherapy programs, and a third semi-synthetic, vinflunine, is in advanced clinical trials. In addition to these five compounds studied in the present work, there are hundreds of other natural and semi-synthetic *Vinca* alkaloids known, although most are not clinically advantageous. The *Vinca* alkaloids are anti-mitotic agents that affect the cellular protein tubulin and bind to a specific site known as the *Vinca* domain located on β-tubulin. While the *Vinca* domain is well established, the specific binding mode of each drug is not. However, there is much insight into the binding mode and this has provided a strong base of information to begin simulations and to make comparisons against. Complicating the issue, however, is the large size of the *Vinca* alkaloids and their complex molecular structure, including a rotatable single bond joining the indole and indoline portions of each compound. The differential geometric and tubulin-binding properties of the drugs are not fully known. In the present work, the projection of the potential energy surface on the major torsional angle was calculated at the semi-empirical AM1 level, through *in vacuo* geometry optimizations. QM/MD simulations were performed, with the drugs at the AM1 level, of each *Vinca* alkaloid free in TIP3P water, and also bound to β-tubulin. A single equilibrium structure, resembling a known crystallographic vinblastine structure [1], for the free drugs was found. Further, the 1Z2B crystal structure [2] of vinblastine bound to tubulin appears to be a valid starting point for simulations of all five *Vinca* alkaloids studied here.

1. Introduction

Since the isolation of vinblastine (VLB) (Fig. 1) from *Catharanthus rosea* in the 1950s [3], the *Vinca* alkaloids have become an important part of modern cancer chemotherapy. At least 130 compounds have been isolated from *C. rosea*, and about 40 of them are similar in structure to VLB. There has been great effort expended over the past several decades to test other compounds isolated from the periwinkle plant. However, currently only two natural *Vinca* alkaloids are approved for clinical use: VLB and vincristine (VCR) (Fig. 1). Numerous semi-synthetic compounds based on the structure of VLB have also been studied in the past. Two such semi-synthetics are clinically used, vindesine (VDE) (Fig. 1) [4] and vinorelbine (VNO) (Fig. 1) [5,6], and a third, vinflunine (VFL) (Fig. 1), has shown promising and unique results in clinical trials [7].

The *Vinca* alkaloids demonstrate anti-mitotic activity in cancer cells that causes apoptosis. This effect is likely through binding to tubulin and interference with microtubule dynamics [8]. Microtubules, comprised of the protein tubulin, are a structural component of the cellular cytoskeleton. A crucial role of microtubules is to provide mechanical force required as part of the mitotic spindle apparatus during chromosome segregation in mitosis. Tubulin is primarily present in microtubules in two different forms: α tubulin and β-tubulin; these forms (coded by different genes) almost always exist in a stable non-covalent α-β heterodimer. The *Vinca* alkaloids are generally known to bind in a rapid and reversible fashion to a high-affinity site on β-tubulin [2,8–12] termed the *Vinca* domain. The photochemical studies by Rai [10] and Chatterjee [11] provide evidence to support the binding mode in the recently determined crystal structure of VLB bound to tubulin [2]. Each *Vinca* alkaloid mentioned here is known to bind with a different affinity [13] and clinically have different uses, toxicities, and effect spectra [14].

* Corresponding author.
E-mail addresses: ebkelly@ualberta.ca (E.B. Kelly), jackt@ualberta.ca, jtus@phys.ualberta.ca (J.A. Tuszynski), mariusz.klobukowski@ualberta.ca (M. Klobukowski).
[1] Present address: Faculty of Law, University of Victoria, Victoria, British Columbia V8W 3H7, Canada.

1093-3263/$ – see front matter.
doi:10.1016/j.jmgm.2011.06.005

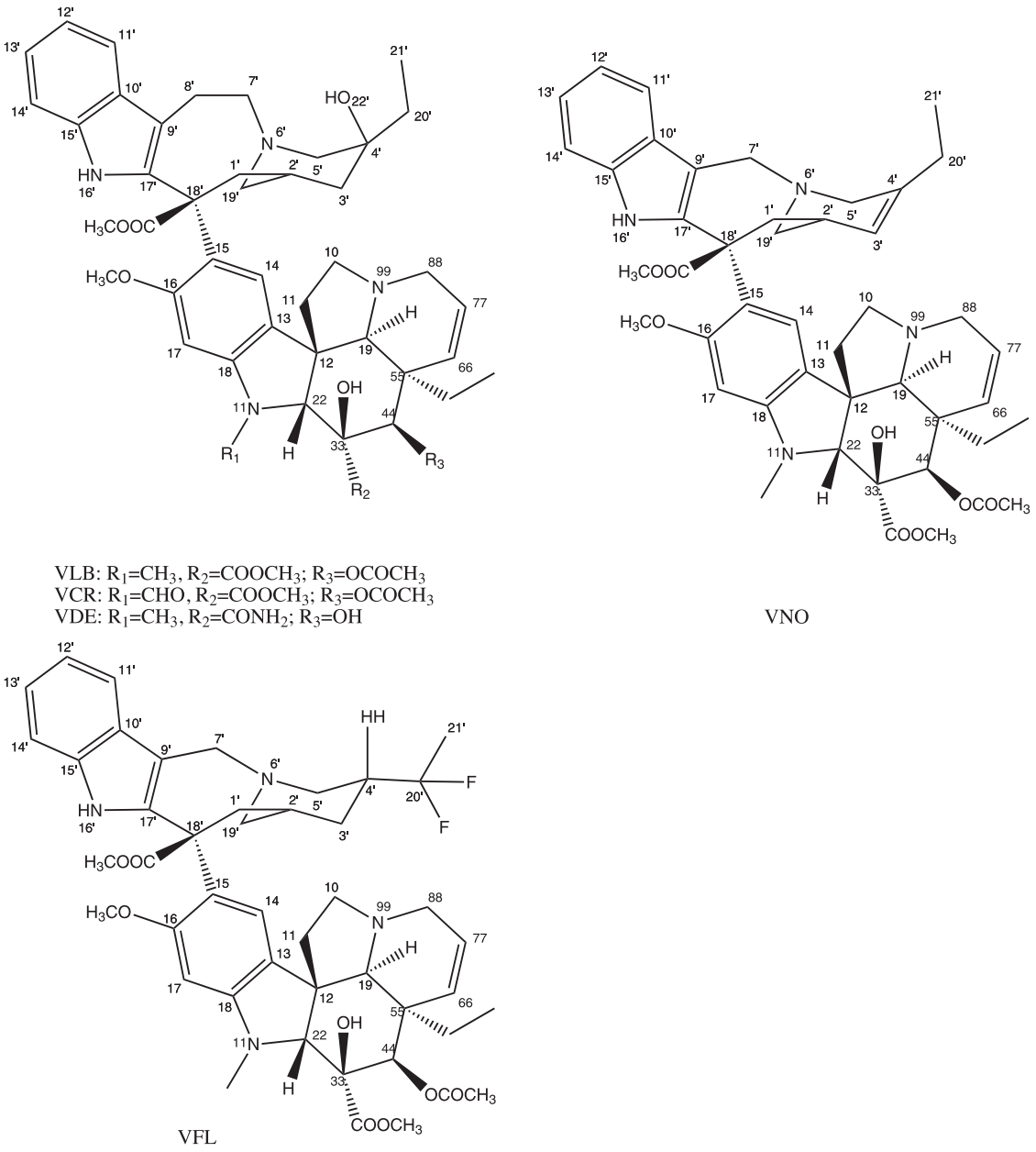

Fig. 1. The chemical structures of vinblastine (VLB), vincristine (VCR), vindesine (VDE), vinorelbine (VNO), and vinflunine (VFL).

The "top" portion of the *Vinca* drugs is an indole moiety and will be referred to with primed atom numbers; the "bottom" portion is an indoline moiety and will be referred to with unprimed atom numbers. There have been a variety of structural and geometric studies performed on the *Vinca* alkaloids. Of particular interest is the C17′–C18′–C15–C16 dihedral angle (referred to as the 'main dihedral angle' about the single C–C bond joining the top and bottom portions of the drug (Fig. 1). Torsion about this bond may lead to an altered molecular surface and affect properties such as binding to tubulin. Major contributions to studies of the structure of *Vinca* alkaloids are summarized below.

In 1965, Moncrief and Lipscomb obtained an X-ray crystal structure of VCR methiodide [17]. They found the main dihedral to be approximately 160°. A similar crystal structure for VLB was not found: the crystal structure of VLB has proven challenging to discover. In 1983, 2D-NMR studies of VLB separately in both benzene and dichloromethane at room temperature were reported by Hunter [18]. The main dihedral was estimated to be in the range of 140–170°. No explanation is given of how the structural analysis and modeling were done, and it is assumed that no computational models were constructed. In 1992, Gaggelli [19] performed a 2D-NMR proton and ^{13}C NMR study of VLB in aqueous solvent. A computational model was constructed at the MM2 [20] force field level and an energy-minimized structure was found under NMR distance restraints. The main dihedral angle was found to be approximately 180°. In 1995, Andrews [21] presented a 2D-NMR study of 3′-4′-anhydrovinblastine in trichloromethane at 263 K. Only peak assignments were made from the NMR data and distance restraints were not discussed. The MacroModel 4 [22] program was used to perform a Monte-Carlo search for minimum geometry structures at the MM3* [23–25] force field level. The lowest energy structure found was one with a main dihedral angle of 37° and the second lowest energy structure had an angle of 207°. These structures were discussed in terms of the NMR data and the 207° structure was considered to be in the closest agreement with experiment. In 2000, Bau and Jin [1] applied new crystallization

techniques to VLB and found an X-ray crystal structure of vinblastine sulfate at 173 K. The geometry of this structure was very similar to Moncrief's structure of VCR from 35 years earlier. The main dihedral angle in Bau and Jin's structure was 162°.

In a recent paper [26], the effect of VLB on microtubule geometry was studied with molecular mechanics methods implemented in the AMBER code [27] employing the FF03 and GAFF force fields; the role of amino acids at the binding interface was analyzed using computational alanine scanning technique [28].

The rational design of new *Vinca* alkaloid drugs is an important goal, as apparently minor changes in chemical structure can lead to large changes in binding to tubulin and clinical profiles, thus suggesting the potential for development of improved *Vinca* alkaloid drugs. However, a direct comparison of the geometric and conformational properties of the most important *Vinca* alkaloids is not available, making rationalization of the effects of functional group changes difficult. Thus, we present here a direct computational comparison of VLB, VCR, VDE, VNO, and VFL using the semi-emperical AM1 level of theory both in free solution conditions and with compounds bound to tubulin.

The binding mode of VLB to tubulin has been the object of investigations for many years. Studies have shown that VLB binds to tubulin ends with high affinity but also binds with a much lower affinity to tubulin sites located along the surface of the microtubule cylinder [9,29,30]. Approximately 16–17 high-affinity binding sites have been determined to exist per microtubule, which are located at MT ends. They are responsible for the well-known kinetic suppression effects of VLB at low concentrations (sub-micromolar). The binding of vinca alkaloids to the low affinity binding sites on the MT surface is believed to be responsible for the depolymerization of MTs at high drug concentrations. At high concentrations, VLB binds to MTs which results in their depolymerization. However, at low concentrations, VLB is thought to bind to MT tips and suppresses their dynamic instability, leading to MT stabilization [31]. This may be a result of VLB's ability to maintain the tubulin dimer at the end of the growing MT in a slightly bent conformation [32]. If the tip of a protofilament was maintained with a slightly bent conformation, due to the positioning of VLB between the dimers, then at low enough concentrations a small amount of drug bound to the end of the MT would mimic the presence of a GTP cap, thereby resulting in MT stabilization. To further emphasize the importance of the high affinity binding site with the exposed β-tubulin at the plus end of a microtubule, Panda [33] demonstrated that VLB exerts strikingly different effects on the dynamics and polymer mass at the plus and minus ends of microtubules. At concentrations between 0.1 and 0.4 mM, the drug strongly depolymerizes microtubules at minus ends, whereas it does not significantly depolymerize microtubules at plus ends.

In terms of the specific residues involved in these two distinct modes of action, only the high affinity binding sites have been determined so far and we discuss this below based on crystallographic data and our own analysis. Several crystallographic structures of tubulin are now available from the RCSB Protein Data Bank (PDB) [32,34,35]. The first tubulin structure, 1TUB, was crystallized as a flat Zn^{2+} induced sheet using docetaxel as a stabilizing agent [36] and was later refined and superseded by 1JFF, in which paclitaxel was utilized as a stabilizing agent [15]. Similarly, 1TVK was generated using epothilone A, which binds at the taxane binding site [37]. Additional structures use a stathmin-like domain to produce crystals, e.g. 1FFX [38]. Two higher resolution structures, 1SA0 and 1SA1 were obtained for the colchicine- and podophyllotoxin-bound complexes of tubulin [39]. Both the colchicine and VLB binding sites are observed in 1Z2B [2]. In the latter case, VLB was shown to bind at the inter-tubulin dimer interface, resulting in the net reduction of polymerized tubulin concentration [2].

Table 1
Changes of residues between tubulin isoforms in the locations forming interactions with vinblastine.

Isoform	Position			
β III				Thr218-Ala
β VII		Phe212-Ser		Thr218-Pro
β VIII	Ser172-Leu	Phe212-Ser	Arg213-Lys	Thr218-Pro

Gigant et al. identified several important interactions between β-tubulin and VLB [2]. First, several contacts with residues Val175, Asp177, Tyr208 and Phe212 were shown to be in agreement with previous photoaffinity labeling experiments that identified residues 173-211 to be involved in VLB binding. Of these four residues, Asp177 was shown to become displaced from a position close to the bound GTP molecule to a position that is near VLB. Residue Tyr222 was also identified as becoming captured between the base of the bound GDP and the D' ring within VLB.

We assume, therefore, the VLB binding site is comprised of only two domains that contain residues 172–177 and 208–225. This produces a set of only 24 residues within the 6 Å cutoff from VLB. Of these 24 residues, only four positions show any variation within each of the tubulin isoforms [40]. This places this binding site's variability clearly in the center between that of the paclitaxel and colchicine binding site. We have identified that differences within the VLB binding sites occur over the same β-tubulin isoform range as that of the paclitaxel binding site, encompassing β III, β VII, and β VIII (see Table 1). However, only residue Phe212-Ser within this set correlates directly with any of the positions identified by Gigant [2]. This substitution occurs on the periphery of the vinblastine binding site and in combination with Arg213-Lys could lead to structural differences within the H6–H7 loop. The β VIII substitution, Thr218-Pro is likely to have a dramatic effect on the terminus of the H6 helix, potentially resulting in its extension and displacement. Both isoforms β VII and β VIII demonstrate significant changes within this H6–H7 loop. It is also interesting to assess the known effects of tubulin mutations within the Vinca binding site [41]. A single mutation at position S172 resulted in an increase in MT stability and a resistance to the hemiasterlin HTI-286 which shares a binding region on tubulin with the vinca alkaloids [42].

2. Computational methodology

Inspection of the structure of the *Vinca* alkaloids reveals that the main (C17′–C18′–C15–C16) dihedral angle is of great interest: it connects two relatively large groups and torsion about this bond will result in quite different molecular shapes. This is relevant for a number of reasons, but perhaps the most important is that as both top and bottom portions of the *Vinca* alkaloids are apparently involved in binding to tubulin, the binding interfacial regions may be different at different main dihedral angles. The projection of the potential energy surface at the semi-empirical AM1 level of each *Vinca* alkaloid onto the main dihedral angle has been calculated in an effort to understand the rotational properties about this angle.

2.1. Potential energy as function of main dihedral angle

Starting coordinates for VLB were taken from Bau and Jin's crystal structure [1]. These coordinates were used as input in the SPARTAN[43] molecular building environment on an Apple Power-Mac G5 Quad 1.9 GHz computer. Structures of VCR, VDE, VNO, and VFL were created by mutating the VLB structure at the required functional groups and by deleting the C8′ atom in the latter two cases. Each structure was then quickly optimized at the MMFF [44–48] level in the SPARTAN building environment. For each drug, 72 models were created: one for each of the angles between 0° and

355° at 5° increments. The main dihedral angle was restrained at each angle, and a Monte Carlo conformer search was performed at the MMFF level for each dihedral angle. A Monte Carlo search was not performed on VFL as the SPARTAN program was found to erroneously reverse the stereochemical configuration at the C18′ position during the search – instead, the structures of VFL were manually prepared based on the results from the other four drugs. The coordinates resulting from the Monte Carlo search were then used as input to the PC-GAMESS program [49] (which is partially based on the GAMESS-US source code [50]) and, keeping the main dihedral restrained at the same 5° increments, *in vacuo* geometry optimizations were performed at the semi-empirical AM1 level. The PC-GAMESS calculations were performed on a cluster of AMD Athlon 2.0 GHz computers. Restraints were imposed using the `$zmat` keywords `IFZMAT`, `FVALUE`, and by setting `AUTOFV = .false.`, which is a feature unique to PC-GAMESS in the GAMESS family of programs. The calculations used automatically generated delocalized internal coordinates. The Hessian matrix was calculated at the initial optimization step, and then subsequently every 10 steps afterwards, with the BFGS Hessian update method [51] performed at each step in between. SCF density convergence of less than 1×10^{-5} a.u. was required, and in the Rational Function Optimization (RFO) [52] routine a geometry convergence criterion of 1×10^{-4} hartree bohr^{-1} (for the largest component of the gradient) was used. The energies of the optimized structures, converted to units of kcal mol^{-1}, were plotted against the dihedral angle and this is the projection of the potential energy surface on the torsion of the main dihedral angle. The graphs for each of the five drugs displayed 'spikes' and 'plateaus' of unexpectedly high energy. It is likely that these high energy regions were the result of the systems becoming caught in local energy minima. To remedy this, the structures from neighboring low energy angles were shifted in their main dihedral angles by five or ten degrees to the angles of the high energy structures. These shifted structures were then optimized again. This procedure allowed for the lowering of most unusually high energy regions, leaving a smoother surface, although some minor insignificant spikes were still present.

2.2. QM/MD simulations of free drugs

Again using the SPARTAN program, the same starting structures of each drug used in the geometry optimizations were used. An unrestrained Monte Carlo search was performed at the MMFF level on each drug, and the 20 structures with the lowest energy were kept. The resulting structures were binned by main dihedral angle in groups of 10° width and the lowest energy structure from each bin was chosen to be used in an MD simulation. Additionally, several structures were chosen from the geometry optimized structures in an effort to better represent certain areas of the torsional potential energy surface. For VFL, no Monte Carlo search was performed due to the tendency of a SPARTAN Monte Carlo search to reverse the stereochemistry at the C18′ site. All of the structures chosen for VFL were taken from its torsional potential energy surface structures. As there are multiple structures simulated for each drug, the notation of VLB_N, where N is an index to describe the starting conformation, will be adopted when discussing these QM/MD simulations. The main dihedral angles for the six VLB structures VLB_1 through VLB_6, respectively, are: 205.3°, 154.9°, 311.3°, 37.6°, 175.0°, and 120.0°. The five VCR structures have angles: 153.1°, 202.0°, 311.9°, 165.4°, and 36.3°. The seven VDE structures have angles: 205.0°, 155.2°, 311.1°, 168.2°, 37.5°, 315.4°, and 120.0°. The three VNO structures have angles: 195.4°, 11.1°, and 315.0°. The four VFL structures have angles: 195.0°, 20.0°, 285.0°, and 100.0°. The `solvatebox` command from the TELEAP program of the AMBER[27] suite was used to solvate each drug molecule by periodically placing pre-equilibrated boxes of TIP3P water around the solute drug. Water molecules that were placed within the van der Waals radius of any solute atom were automatically removed. Exactly 2000 water molecules were added to each simulation box.

Born-Oppenheimer QM/MD simulations were performed using the SANDER program from the AMBER 9 suite [27]. The leap-frog integrator was used to propagate the system in molecular dynamics. QM forces were calculated using an SCF procedure. An SCF cycle was considered converged when an energy convergence criterion of 1×10^{-8} kcal mol^{-1} and a largest element-wise change in density matrix criterion of 5×10^{-10} were both met. Electrostatic cutoffs were used as follows: any two MM atoms within 10 Å of each other interacted with each other, an MM atom within 8 Å from the QM boundary interacted with the QM region, and all atoms within the QM region interacted with each other through the Hartree-Fock equation. A Particle Mesh Ewald method (PME) modified for QM/MM systems [53] was applied to long-range electrostatics. The Langevin thermostat was used in MD simulations to control the temperature. The SHAKE [54] algorithm was used to constrain bond lengths: this was applied only to bonds involving hydrogen and all such bonds (solute and water) were restrained to equilibrium bond lengths at all times during MD simulations.

Before MD simulations were started, brief geometry optimizations were performed. In an effort to speed up the calculation, the solute was represented with the Generalized Amber Force Field (GAFF) [55] and AM1-bcc charges.[2] Periodic box boundary conditions were used with the box volume held constant. In a first step, the solute atoms were all restrained to their original positions using parabolic energy penalties with a force constant of 100 kcal/(mol Å^2). The steepest descent algorithm was used for 250 iterations, and then the conjugate gradient method was used for 750 iterations. A second step was subsequently performed, with no positional restraints on the solute, for 500 iterations of steepest descent and then 2500 steps of conjugate gradient minimization.

The solvent was then 'warmed' with parabolic restraints on the solute. The force constants used were 20 kcal/(mol Å^2), and the solute was restrained to the coordinates resulting from the previous two stages of energy minimization. The Langevin thermostat was used with a collision frequency of 5 ps^{-1} and a target temperature of 310 K. An integrator time step of 0.5 fs was used and 10,000 steps of molecular dynamics simulation were performed, under periodic box conditions with a constant volume. Next, a further 25,000 steps with a timestep 2 fs were performed for solvent equilibration. The same GAFF/AM1-bcc description of the drugs was applied here in an effort to speed up the process.[3] The optimization, warming, and solvent equilibration stages were all performed on an Apple iMac G5 1.9 GHz computer using the SANDER program.

Next, the entire system was equilibrated, without restraints, at the AM1/TIP3P solute/solvent level of theory. Periodic box conditions were again used, only this time with the use of a barostat to yield a constant pressure of 1 bar. A pressure relaxation time of 2 ps^{-1} and isotropic box scaling were used for pressure regu-

[2] The force-field representation of solute was used mostly with the solute restrained and therefore no geometric differences would result compared to using the slower AM1 method. The GAFF representation was only used unrestrained for a small number of energy minimization steps, therefore the resulting geometry would not be appreciably different than if an AM1 representation had been used. Furthermore, the GAFF force-field was tested and demonstrated to not accurately model the *Vinca* alkaloids, so unrestrained simulation using this force-field would not be advised.

[3] Caution must be exercised when using a force-field method to equilibrate a system for QM/MD simulations as the two methods may describe the system differently and conformational changes may occur during equilibration that would not occur in the molecular dynamics simulation. GAFF/AM1-bcc was used for dynamics simulations only when the solute was restrained.

lation. The collision frequency for the Langevin thermostat was set to 1 ps^{-1} and a temperature of 310 K. A time-step of 2 fs was used over 50,000 steps. Each system was judged to be equilibrated once the potential energy, kinetic energy, pressure, and density of the system reached stable values with no increasing or decreasing drift. This point was typically obtained by the 50 ps mark of the unrestrained equilibration simulation. Exactly the same conditions were used for the production simulations, which were performed for a total of 5 million time steps to give 1 ns of simulation. The full equilibration and production runs were performed on a cluster of 3.06 GHz Intel Xeon processors. Data points were taken every 0.1 ps and analysis of the simulations was performed with the PROCESS_MDOUT.PERL script and PTRAJ utilities from the AMBER suite of programs. Radii of gyration were calculated by the usual formula. In addition to the main dihedral angle, the linear distance between the C4′ atom on the top portion of the drugs and the C10 atom on the bottom of the drugs were calculated. This distance was chosen as an alternative, structure independent, geometric parameter of the main dihedral angle. Both of these atoms are predicted by the 1Z2B structure to be in contact with tubulin in a bound state, thus their relative position may be important. Statistical errors were calculated using the blocking method [56].

2.3. QM/MD simulations of bound drugs

The 1Z2B PDB entry [2] was used as a starting structure for tubulin bound to a *Vinca* alkaloid drug. A model of an exposed microtubule +end, which is the site of most *Vinca* alkaloid binding, was developed from the interior β-tubulin unit, the bound VLB drug, and the GDP molecule in the nearby hydrolyzable nucleotide site. In order to most accurately reflect the conditions of a growing microtubule tip, the GDP molecule was converted, by the TELEAP program of the AMBER suite, to GTP by the addition of an extra phosphate group. The conversion was done according to a minimized template structure of free GTP, and did not affect the existing GDP atoms. Similarly, minimized templates of the *Vinca* alkaloid drugs VCR, VDE, VNO, and VFL were prepared and used to mutate the VLB unit. In an attempt to limit human bias, no manual adjustments were made to the drug conformations. Thus, five systems were prepared: one for each drug, each with GTP.

The simulation procedure used for the tubulin-drug complexes is nearly identical to that used for the free drugs, thus only the differences will be discussed here. The tubulin protein was described by the AMBER FF03 force field [57], and the GTP molecule was described by the force field parameters determined by Meagher [58]. The system was solvated with approximately 16,000 TIP3P water molecules using TELEAP's `solvatebox` command. Randomly chosen water molecules were deleted and in their places 20 Cl^- and 39 K^+ ions were added to bring the system to a net neutral charge and an ion concentration of approximately 100 mM KCl. The remaining water molecules were deleted. The solute and ion system was then resolvated with exactly 16,000 water molecules. All other simulation details and parameters were the same as in the drug-only simulation.

The system was energy minimized first with all solute protein and drug atoms restrained: the drug was described with the same GAFF AM1-bcc parameters as in the free drug simulations. The second minimization stage was performed with most of the system unrestrained, except the drug was restrained again in an attempt to keep the conformation from changing through interaction with the protein. The warming of the solvent was then performed with protein and drug restrained. A solvent equilibration was then performed for a total of 250,000 timesteps which gives a total of 500 ps of simulation time. A full unrestrained equilibration, with the drug described at the AM1 level, was performed for a total of 0.1 ns. The production simulation was performed for 1 ns.

Basic analysis was performed as with the free drug simulations. Additionally, coordinate snapshots were taken 10,000 times (once every 0.1 ps) during the production simulation. The `checkoverlap` command in the PTRAJ utility was used to record all pairs consisting of a drug atom and a protein atom that were within 4 Å of each other. These results were then summed over time and any interaction that was present for more than 5,000 snapshots, or 50% of the 1 ns simulation, in total was considered significant. This analysis was done on an Apple PowerMac G5 Quad 1.9 GHz computer.

3. Results and discussion

3.1. Torsional potential energy surfaces about the main dihedral angle

The potential energy surface projections onto the main dihedral angle of each drug are presented in Fig. 2. Of note are the minor spikes in the 0–100° region of the VLB surface and the spikes near 180° in each of VLB, VCR, and VDE. The plots for VLB, VCR, and VDE are all very similar, each with a global minimum at about 205° and with secondary minima at about 35°, as well. The relative depths of the secondary minima are about 2.5 kcal mol^{-1} in both VLB and VDE, but the depth of this minimum in VCR is about 0.5 kcal mol^{-1}. The VNO and VFL plots are similar to the other three, but with a global minimum at 195° and a secondary minimum at about 20° which is 3 kcal mol^{-1} higher in energy than the global minimum.

As the main dihedral angle is changed about a full rotation, major conformational changes occur in the backbone structure of the top portion. At the minimum energy conformations near 200° and 40° the top portion closely resembles the geometry found by Bau and Jin [1]. In the 300–360° domain, the top portion adopts a conformation that is considerably bent in the middle. The structure at the energy plateau near 100° is similar to the bent conformation near 300° but can become very distorted and even the chair conformation of the piperidine ring is lost. Each of the drugs undergoes these same conformational changes, including VNO and VFL, despite the smaller and less flexible 8-membered ring and the double bond in the piperidine ring of VNO. Of course, the double bond in the piperidine ring of VNO forces that 6-membered ring into a near-planar shape.

Using VLB as an illustrative example, Fig. 3 shows the varying conformations of the top portions of the drugs. The structure (a) for the main dihedral angle of 200° is similar to the one found using X-ray crystallography by Bau and Jin [1] in that the piperidine ring is in a chair conformation and the C18′, C1′, and C8′ atoms are nearly coplanar with the indole moeity. VCR, VDE, and VFL adopt similar conformations near minima of their torsional potential energy surfaces. The structure (b) for 350° differs from the one found using X-ray crystallography by Bau and Jin [1] in that the coplanarity of the indole moeity and C18′ is lost, but the chair conformation of the piperidine ring is preserved. VCR and VDE adopt similar conformations near peaks of their potential energy surfaces. Finally, the structure (c) obtained for the main dihedral angle of 110° is an example of a very distorted, high energy structure of VLB. This structure differs significantly from the one found using X-ray crystallography by Bau and Jin [1] in that the coplanarity of the indole moiety and C18′ is lost and the piperidine ring is distorted out of the chair conformation. Most other high energy structures of the *Vinca* alkaloids adopt a bent conformation.

Several VNO and VFL conformations are shown in Fig. 4. The structure (a) of VNO for the angle of 195° is an example of a low energy, stable conformation of VNO; most structural features found in the VLB crystal structure of Bau and Jin are preserved here. At the angle of 300° structure (b) of VNO is an example of a bent, high energy structure of VNO. The top portion of VNO takes on a more

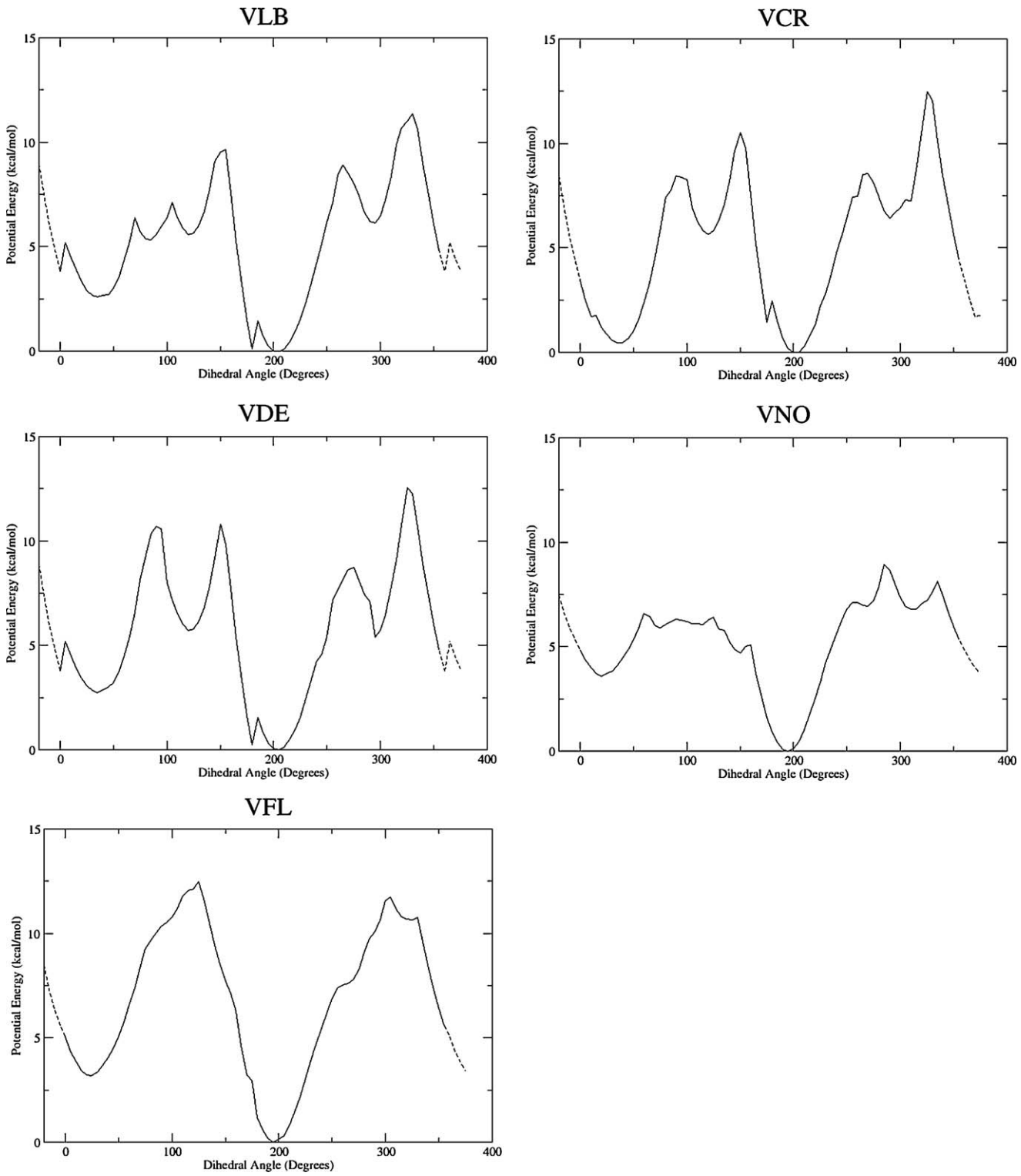

Fig. 2. The projection of the potential energy surfaces of vinblastine (VLB), vincristine (VCR), vindesine (VDE), vinorelbine (VNO), and vinflunine (VFL) onto the C17′–C-18′–C15–C16 dihedral angle. The graph is periodically wrapped in the −20–0° and 360–380° domains (in dotted lines) for increased clarity.

extreme bend at these high energy structures when compared to VLB, VCR, and VDE. Structure (c) for VFL is an analogue of structure (b) of VNO: it is a bent, high energy structure of VFL, with top portion of VFL displaying a more extreme bend when compared to VLB, VCR, and VDE.

The dipole moments calculated in the *in vacuo* AM1 energy minimizations, at several conformations each, of the *Vinca* alkaloids are presented in Table 2.

3.2. QM/MD simulations of free drugs

One simulation for each drug was started very near each of the two minimum energy main dihedral angles found in the 0 K AM1 torsional potential energy surfaces. These simulations remain stable at the starting value of the main dihedral, indicating that the 0 K minimum energy angles are also the equilibrium angles in finite temperature simulations. The other simulations exhibit two types

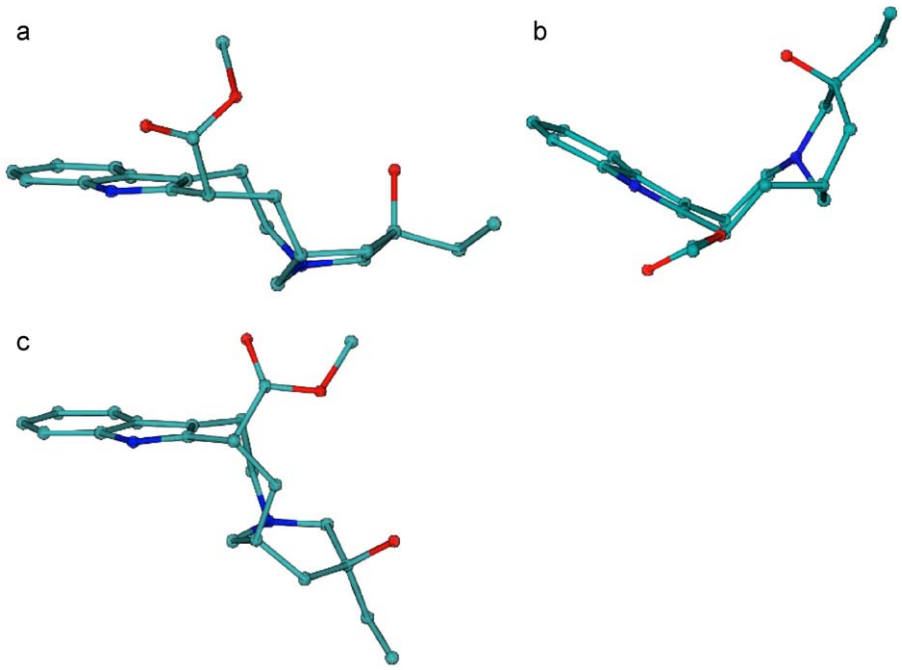

Fig. 3. Top portion of VLB from the AM1 structures optimized for several main dihedral angles: (a) 200°, (b) 350°, (c) 110°. Hydrogen atoms removed for clarity. Carbon C18′ in the 8-member ring is the atom attached to –$COOCH_3$ group. Figure created using VMD [16].

of behaviour: (1) they collapse directly to an equilibrium main dihedral angle; or (2) they eventually collapse to one of the two equilibrium angles, after staying in one or more metastable conformations for up to 0.5 ns. It is of utmost importance to note about these plots that, despite initial variance in structure, each molecule will eventually adopt one of two stable values of the main dihedral. Thus, the results from the simulations started from each of the equilibrium values are the most important. The averaged results of these simulations are presented in Table 3 along with the C4′–C10 distances. Also in Table 3 are averaged radii of gyration, AM1 energies of the solute drug, and overall QM/MM energies of the entire drug and solvent system.

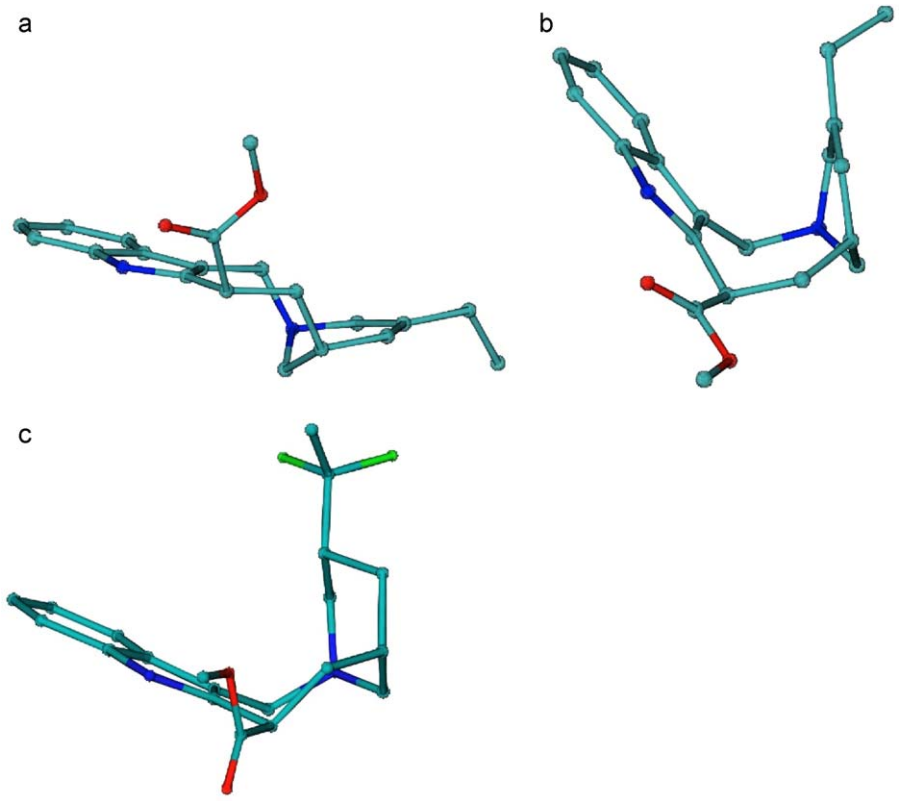

Fig. 4. Top portions of the AM1 optimized structures for several values of the main dihedral angle: (a) VNO for the angle of 195°, (b) VNO for the angle of 300°, (c) VFL for the angle of 325°. Hydrogen atoms removed for clarity. Carbon C18′ in the 8-member ring is the atom attached to –$COOCH_3$ group. Figure created using VMD [16].

Table 2
In vacuo AM1 dipole moments at the minima of the *Vinca* alkaloids. 'Angle' refers to the C17′–C18′–C15–C16 dihedral angle.

Drug	Angle (°)	Dipole moment (D)
VLB	205	2.14
	180	2.67
	195	1.88
	215	2.22
	35	2.88
VCR	200	3.60
	175	5.81
	190	3.64
	215	3.48
	35	5.43
VDE	205	2.88
	180	4.31
	195	2.75
	215	2.87
	35	2.98
VNO	195	2.36
	185	2.23
	205	2.44
	20	3.32
VFL	195	2.60
	185	2.42
	205	2.99
	20	5.85

3.3. QM/MD simulations of bound drugs

The QM/MD simulations of each drug bound to the *Vinca* domain all began in a conformation near the 200° equilibrium structure found in the free aqueous form, as found in the 1Z2B structure. There were no major shifts in the main dihedral angle through the simulation, indicating that the starting structures were essentially stable. The averaged results of these simulations are presented in Table 4 along with the C4′–C10 distances. Also in Table 4 are averaged radii of gyration, AM1 energies of the solute drug, and overall QM/MM energies of the entire drug, protein, and solvent system. The blocking method was, as before, applied to calculate statistical errors. The method failed to converge when applied to the VLB main dihedral angle.

4. Free form *Vinca* alkaloids

4.1. Potential energy surface

The torsional potential energy profiles are likely a result of the distortion of the top drug portion and the flexible 8- or 9-member ring is exactly where the distortion occurs. The bottom half of the drug is much more rigid, due to its polycyclic nature containing smaller rings. Two conformational groups occur due to similarity in the top portions of the drugs: VLB, VCR, and VDE each have the same top structure, but VNO and VFL both have a smaller 8-member ring instead of a 9-member ring. It was theorized by Hunter [18] that the conformation of VLB would not be dependent on side-chain interaction, and this theory appears to be confirmed here: it is distortion of the top portion that gives rise to conformational preference in the *Vinca* alkaloids.

The surfaces presented here were not smooth, as would be expected in a torsional energy profile, but rather jagged with many spikes. The most reasonable explanation is that the spikes originate in the system becoming caught in a local energy minimum and not a global minimum (for the torsional restraint applied), which translates to a fallaciously high energy for that torsional angle. The goal of calculating these torsional energy profiles was to provide a guide for the conformation of the *Vinca* alkaloids. Reasonable effort was taken to smooth the profiles as much as possible. While the energy spikes are not ideal, the results here are sufficiently smooth to satisfy the initial goal: it is clear that one conformation near 200° is strongly preferred. A secondary minimum in the range of 10–40° exists, but is of higher energy and is largely insignificant (see Section 4.3). The observation of this secondary minimum is consistent with the results of [21], where computational modeling found a minimum of VLB at 39°, which was discounted based on experimental data in favour of a minimum at 207°.

4.2. MD simulations

The 0 K potential energy surfaces predict only two stable conformers for each *Vinca* alkaloid. The QM/MD simulations performed follow those predictions very closely: regardless of the starting conformation the structure collapses to one of the two energy minima. The average angles in the MD simulations are within a few degrees of the minima in the 0 K energy surfaces, indicating that solvation and non-zero temperature do not considerably affect the structures predicted by the 0 K minimizations of the *Vinca* alkaloids. Thus, the grouping mentioned above (VLB, VCR, VDE, vs. VNO, VFL) still holds in aqueous MD simulations. The average C4′–C10 distances are all within 1.1 Å of each other, thus the interaction between each drug and the *Vinca* domain is expected to be very similar in each drug as the relative orientation of the tubulin-interacting regions of the top and bottom portions are comparable. The energies of the QM regions, which are the AM1 energies of the drugs alone, were calculated to a low enough error for comparison to be significant.

4.3. Conformation populations

Based on the torsional potential energy projections presented in Fig. 2, it is evident that of the two minimum angle conformations, the conformation at approximately 200° is the preferred conformer

Table 3
The average properties of the *Vinca* alkaloids from 1 ns of QM/MD simulations. Error values, where available, are in parentheses behind each value. 'Angle' refers to the C17′–C18′–C15–C16 dihedral angle, and $r_{C4'-C10}$ is the average distance between atoms C4′ and C10. R_G refers to the radius of gyration. E_{AM1} are AM1 energies are for the ligand only, and PE_{Tot} are total potential energies are for the entire QM/MM system, both in kcal mol^{-1}.

	Angle (°)	$r_{C4'-C10}$ (Å)	R_G (Å)	E_{AM1}	PE_{Tot}
VLB_1	207.9 (0.8)	7.78 (0.04)	5.4 (0.005)	−192.6 (0.4)	−19096 (4)
VLB_4	38.8 (1)	9.64 (0.12)	5.5 (0.013)	−188.5 (0.4)	−19099 (3)
VCR_2	207.6 (0.8)	7.27 (0.10)	5.4 (0.008)	−226.5 (0.4)	−19124 (3)
VCR_5	36.4 (0.9)	9.03 (0.08)	5.5 (0.02)	−222.7 (0.5)	−19122 (3)
VDE_1	208.8 (1.3)	7.93 (0.03)	5.2 (0.004)	−120.6 (0.4)	−19011 (3)
VDE_5	39.4 (0.8)	9.66 (0.06)	5.3 (0.006)	−117.8 (0.4)	−19015 (4)
VNO_1	197.0 (0.7)	8.07 (0.04)	5.4 (0.006)	−122.5 (0.4)	−19023 (3)
VNO_2	16.6 (0.7)	9.22 (0.05)	5.4 (0.01)	−119.2 (0.4)	−19020 (3)
VFL_1	198.1 (0.7)	8.30 (0.04)	5.4 (0.004)	−243.3 (0.4)	−19140 (3)
VFL_2	23.5 (1.1)	9.42 (0.08)	5.4 (0.009)	−239.2 (0.4)	−19142 (4)

Table 4
The average properties of the *Vinca* alkaloids bound to β-tubulin from 1 ns of QM/MD simulations. Error values, where available, are in parentheses behind each value. 'Angle' refers to the C17′–C18′–C15–C16 dihedral angle, and $r_{C4'-C10}$ is the average distance between atoms C4′ and C10. R_G refers to the radius of gyration. E_{AM1} are AM1 energies for the ligand only, and PE_{Tot} are total energies for the entire QM/MM system, both in kcal mol^{-1}.

	Angle (°)	$r_{C4'-C10}$ (Å)	R_G (Å)	E_{AM1}	PE_{Tot}
VLB	211.4	7.63 (0.05)	5.3 (0.014)	−194.2 (1.2)	−166531 (40)
VCR	201.6 (0.7)	8.29 (0.05)	5.4 (0.006)	−241.0 (0.8)	−166605 (30)
VDE	205.1 (0.4)	7.70 (0.03)	5.1 (0.003)	−131.9 (0.5)	−166471 (30)
VNO	195.6 (0.9)	7.94 (0.04)	5.4 (0.003)	−136.7 (0.6)	−166452 (20)
VFL	197.4 (0.6)	8.12 (0.06)	5.4 (0.011)	−247.2 (0.5)	−166575 (16)

as its energy is lower. However, finding the relative populations of the two conformers for each drug will be informative. Assuming the Boltzmann distribution of states, the relative probability between the two is given by:

$$\frac{N_1}{N_2} = e^{(E_2-E_1)/k_B T} \quad (1)$$

where N_1 and N_2 are the populations of the primary and secondary conformers, respectively, E_1 and E_2 are their energies, k_B is the Boltzmann constant, and T is the absolute temperature. If the *in vacuo* 0 K potential energies are used, for each drug except for VCR, the 200° conformation will be present almost exclusively at 310 K. Using the 0 K potential energy difference, the secondary conformation of VCR will be populated by approximately 20% of the VCR molecules in aqueous solution. However, the averaged AM1 energies from the QM/MD simulations of the *Vinca* alkaloids in TIP3P water must be considered. The energy differences between conformers in the MD simulations are approximately the same as in the 0 K energy surfaces, except for VCR, where the secondary conformer has a much higher energy than the primary. The AM1 simulations then predict that each *Vinca* alkaloid will be present almost exclusively in the primary conformation near a main dihedral angle of 200°.

4.4. In vacuo dipole moments

Table 2 shows that primary minimum structures all have dipole moments of about 2 D, with the exception of VCR which has a dipole moment of 3.6 D. This difference may be due to the previously discussed inaccuracy in the primary minimum of VCR. Even if the value for VCR were accurate, each of the drugs may be described as polar, but not very polar. This is shown in the fact that the drugs are characterized by fairly low water solubility unless in acidic conditions. The similar, and moderate, dipole moments indicate that relevant properties of the drugs, of particular interest being cell membrane transport, should be analogous.

Of interest is how VFL is not significantly more polar than the other drugs, despite the presence of two very electronegative fluorine atoms. This is explained by examining the availability of electron density near the fluorine atoms. The fluorine atoms are bound to an ethyl group that is attached to a singly-bonded organic ring. The absence of lone pairs, multiple bonds, and conjugation in this region means that there is little free electron density to move towards an electronegative region of the molecule; despite being highly electronegative, the fluorine atoms have no free electron density to attract. Even though the fluorine atoms of VFL do not affect the global electrostatic properties of the molecule, this is not to say that the flourine atoms will not affect the local properties. In particular, the interaction with tubulin may be altered, especially in light of the evidence showing that this region is buried when bound to tubulin: Rai's study [10] using Ant-VLB and Gigant's crystal structure [2] both show this.

5. The *Vinca* alkaloids bound to β-tubulin

5.1. MD simulations

The 1Z2B crystal structure [2] used as starting coordinates for the MD simulations of all five *Vinca* alkaloids contains VLB in a conformation (main dihedral is 213°) similar to the equilibrium conformers found in the previously discussed MD simulations. This is a good indication that the 1Z2B structure is a reasonable starting point for studies of the *Vinca* alkaloids bound to tubulin. The 1Z2B structure shows a binding mode consistent with the fluorescence studies of Rai [10] and Chatterjee [11]: the the C4′ atom is buried and the C4 functional group is solvent exposed. The main dihedral angles in the simulations are all near their free form values, and cover a slightly broader range of about 16°. The C4′–C10 distances are also similar, but their range is smaller than for the free drugs: only 0.7 Å. Visual inspection of MD trajectories shows that the important features of the Bau and Jin crystal structure [1] including the chair conformation of the piperidine ring and near co-planarity of the indole and 8- or 9-membered rings in the top portion are present. The radii of gyration were also all comparable to the free form values. The AM1 energies were calculated to a low enough error to be significant. Further discussion will be found in the next section.

5.2. Drug–protein pair-wise interactions

Fig. 5 presents the most common pair-wise atomic interactions between the drug and protein in the bound form MD simulations. Code numbers for the pair interactions are shown in Table 5.

This study is by no means an exhaustive examination of the interactions present, but it was intended to provide insight towards how the *Vinca* alkaloids interact with β-tubulin and how the binding differs between the drugs based on the differential molecular structures.

Several interactions appear in most, if not all, drug simulations. The C11 methylene atom interacts with the carbonyl O of the backbone of Lys174 (code = 8) in all drugs except VNO – this is expected to be an unfavourable apolar-polar interaction. The side-chain hydroxyl group of Tyr208 interacts with both the benzene C17 atom (code = 22) and C33 (of the C16 formyl group, code = 24) in all drugs – this is expected to be favourable. Also of note is the interaction between the Tyr208 hydroxyl and C22 (attached to the N1 atom, code = 23) in VLB, VCR (in a formyl group), and VDE. The Tyr208–C22 (code = 23) interaction is interestingly absent in VNO and VFL, despite the fact that these drugs are identical in the bottom portion to VLB. Similarly, the hydroxyl O22′ interactions with the Pro220 backbone oxygen (code = 37) are present in VLB, VCR, and VDE, but this atom is absent in VNO and VFL. Also, O22′ interacts with the C-α of Thr221 (code = 44) in VCR and VDE in a potentially unfavourable interaction.

In addition to Tyr208, C22 also interacts with Lys174 (code = 9) in VLB and VDE. The C22 atom is of relevance due to the observation made by Magnus [59] that VLB, and not VCR, can act as a methylating agent of cysteine residues through C22. The only cysteine

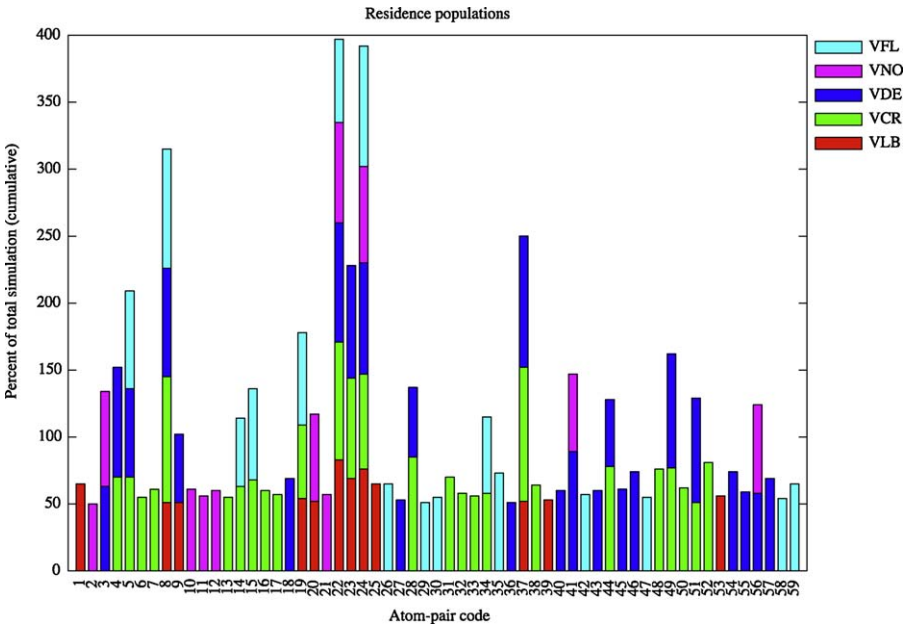

Fig. 5. The atom-pair interactions between bound drug and tubulin. The values are residence populations as a percentage of the total simulation, displayed cumulatively. Drug atom names are shown in Fig. 1 and in footnotes to Table 5.

residue known to be in the *Vinca* domain is Cys211, near Tyr208. While an interaction between C22 and Cys211 is not demonstrated here, it remains possible that a rearrangement of VLB in the binding domain may initiate such an interaction, thereby making methylation possible. However, since Cys211 is shown to interact with the C21′ atom of an ethyl group (code = 25) which is buried deep inside the protein, a C22–Cys211 interaction is not likely, and Magnus's prediction may not be applicable.

The O34 atom is unique to VCR and is in the formyl group attached to N1. This atom appears to be of at least moderate importance through its interactions with Lys174 (code = 6). The conversion of the C22 methyl group in the other drugs to a formyl group in VCR may not affect the C22 interactions in VCR, though, as is seen in the Tyr208 hydroxyl interactions with C22 (code = 23) in VLB, VCR, and VDE. The two ester groups at C3 and C4 in VLB undergo major reductions in the conversion to VDE. However, none of the deleted or added atoms were involved in any significant interactions – this region of the *Vinca* alkaloids does not appear to interact with β-tubulin. Also, the C7′ and C8′ atoms of the 8- or 9-membered ring in the top portion do not interact directly with β-tubulin, making the ring shortening in VNO and VFL of no consequence in this fashion. This ring shortening may have direct consequence through conformational effects, though. The C3′–C4′ double bond in VNO may have some effect on binding compared to

Table 5
Code numbers for the atom-pair interactions between bound drug and tubulin. Please refer to Fig. 1 and the footnotes below for drug atom names. Protein atom names are from the standard AMBER FF03 force field.

Atom pair	Code	Atom pair	Code	Atom pair	Code
Gln11(CB)–C21′	1	Tyr208(OH)–C16	21	Thr221(C)–C21′	41
Pro173(C)–C10	2	Tyr208(OH)–C17	22	Thr221(C)–F2[f]	42
Pro173(O)–C10	3	Tyr208(OH)–C22	23	Thr221(CA)–C21′	43
Pro173(O)–C11	4	Tyr208(OH)–C33[b]	24	Thr221(CA)–O22′	44
Lys174(C)–C11	5	Cys211(CB)–C21′	25	Thr221(N)–C21′	45
Lys174(CA)–O34[a]	6	Thr218(O)–C26′[c]	26	Thr221(O)–C21′	46
Lys174(CD)–O34	7	Pro220(C)–C21′	27	Thr221(O)–F2	47
Lys174(O)–C11	8	Pro220(C)–O22′	28	Tyr222(CE1)–C20′	48
Lys174(O)–C22	9	Pro220(CD)–C26′	29	Tyr222(CE2)–C5′	49
Lys174(O)–C4′	10	Pro220(CD)–O25′[d]	30	Tyr222(CE2)–C20′	50
Lys174(O)–C5′	11	Pro220(CG)–C33	31	Tyr222(CZ)–C5′	51
Lys174(O)–C19′	12	Pro220(CG)–O32[e]	32	Tyr222(CZ)–C20′	52
Val175(C)–C11	13	Pro220(O)–C1′	33	Tyr222(N)–C7′	53
Val175(N)–C11	14	Pro220(O)–C4′	34	Tyr222(N)–C20′	54
Val175(O)–C10	15	Pro220(O)–C7′	35	Tyr222(N)–C21′	55
Val175(O)–C11	16	Pro220(O)–C21′	36	Tyr222(OH)–C5′	56
Asp177(CB)–C8	17	Pro220(O)–O22′	37	Leu225(CD1)–C21′	57
Asp177(OD2)–C8	18	Pro220(O)–O25′	38	Leu225(CD1)–F1[g]	58
Tyr208(CD2)–C3′	19	Thr221(C)–C5′	39	Leu225(CD1)–F2	59
Tyr208(CE2)–C3′	20	Thr221(C)–C20′	40		

[a] O34 is only present in VCR, it is the oxygen atom of the N1-formyl group.
[b] C33 is the C18′ formyl carbon.
[c] C26′ is in the alcohol portion of the C18′ ester group.
[d] O25′ is in the alcohol portion of the C18′ ester group.
[e] O32 is the C18′ formyl carbon.
[f] F2 is present only in VFL and is attached to the C4′ ethyl group.
[g] F1 is present only in VFL and is attached to the C4′ ethyl group.

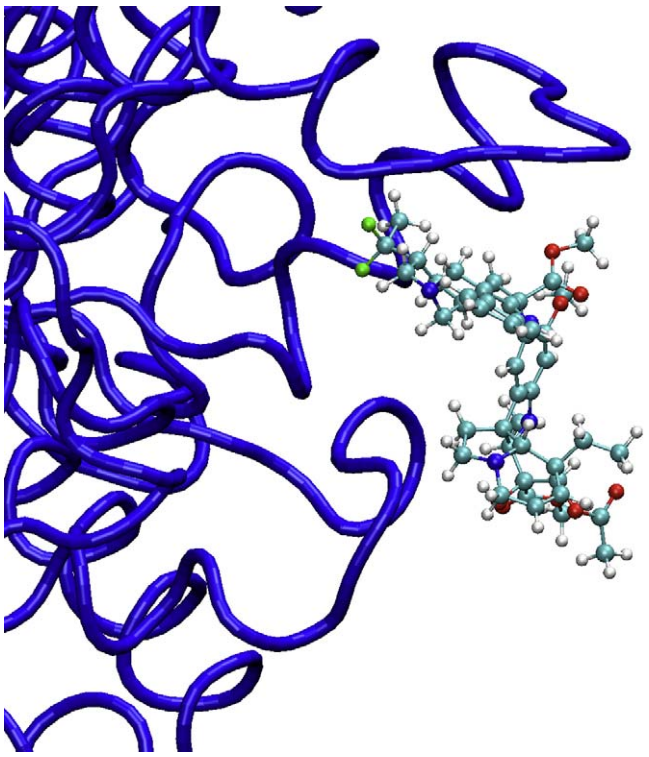

Fig. 6. A snapshot of VFL bound to the *Vinca* domain on β-tubulin. The indole ethyl group, which is the site of the two fluorine adducts (shown in bright green), is the only portion of the drug to be buried into the protein. Figure created using VMD [16].

the singly bonded analogues in the other drugs, as is evidenced in the interactions with Lys174, Tyr208, and Pro220. The most exotic conversion in the five *Vinca* alkaloids studied here is the addition of two fluorine atoms on the C4′ ethyl group of VFL. This region of the drug is very important in the binding mode studied here. As might be expected, these atoms do participate directly in drug-protein interactions, shown in Fig. 6. Both the backbone of Thr221 and side-chain of Leu225 are involved.

As shown in Table 1, the *Vinca* domain has several sites for isotype differences contained within it [40]. It is worth noting that only one significant interaction between a drug bound to β-tubulin was found to involve the mutation sites. This interaction is between VFL's C18′ ester group and the backbone of Thr218, which is where the β III, β VII, and β VIII isotypes (using the previously introduced notation [40]) exhibit different amino acids in identical locations. This interaction may be important in the action of VFL. However, it is an interaction with the backbone of the residue, not the side-chain, so side-chain differences may not affect this interaction. Overall, the design of isotype specific *Vinca* alkaloids may require more subtle analysis than direct atom–atom interactions. While the interaction residues identified here are consistent with previous enumerations of the *Vinca* domain[4] the simulations performed here suggest that the 11th residue in β-tubulin (denoted as β11), while not previously identified as part of the *Vinca* domain, should additionally be included in the binding domain.

It has been experimentally shown that point mutations at Pro173 or at Cys211 are linked to VLB drug resistance [41]. The mutation of Pro173 to Ala induces destabilization of microtubules [60] and the mutation of Cys211 to Phe is found in cells resistant to Colchicine and VLB [61]. Significant contacts between the C10 and C11 atoms of VCR, VDE, and VNO were found to occur with Pro173 (code = 2, 3, and 4) in the 1 ns MD simulations of the drugs bound to β-tubulin. Additionally, the C21′ atom of VLB was found to have significant contact with Cys211 (code = 25). The contact between VLB and Cys211 is of special interest here since the indole ethyl group in the Vinca drugs has been the target site for many synthetic Vinca derivatives, including VFL, and this ethyl group is shown to be buried in the protein. The interaction between Cys211 and VLB is an apolar-apolar interaction between the drug and the side chain methylene group. Introduction of a bulkier apolar Phe side chain at this important site may cause steric-interaction-based inhibition of drug binding and thus confer resistance. *Vinca* derivatives with an *n*-propyl group in place of the ethyl group are up to 10 times less effective at inhibiting microtubule growth [62]. This may occur through a similar unfavourable steric interaction at this important site of drug–protein interaction.

5.3. Comparison of bound to free form of drugs

The equilibrium main dihedral angles of the free *Vinca* alkaloids are all very similar to the angles observed in the bound form. The largest difference is of 6.0° in VCR. With the exception of a 1 Å difference in VCR, the C4′–C10 distances are also very similar in free and bound forms, differing by at most about 0.2 Å. With the possible exception of minor rearrangements of functional groups, these measures indicate that the gross conformation of each *Vinca* alkaloid is the same bound as it is free. As no major reorientation of the *Vinca* alkaloids is needed in order to bind, this suggests a simple one- or two-step binding mechanism. A one step mechanism would simply be a collision of the *Vinca* alkaloid surface with the protein surface. A two step mechanism may involve the collision and binding of either the top or bottom portion of the drug followed by the interaction and binding of the other portion.

The AM1 energies are all lowered in the bound form compared to their equilibrium free form, in VLB by only the small amount of about 2 kcal mol^{-1} and up to about 16 kcal mol^{-1} in the case of VNO. This is indicative of a stabilization of the *Vinca* alkaloids upon binding. Broader energy difference measurements, such as protein deformation energies, drug desolvation energies, or overall binding energies or enthalpies are not possible within the simulations performed. The AM1 energy decrease upon binding can be seen to indicate that binding is favourable. As no major conformational changes occur in the *Vinca* alkaloids upon binding, it can be hypothesized that the AM1 energy decreases are due to interaction with tubulin. This may be through the formation of favourable polar-polar (or non-polar-non-polar) functional group-side-chain interactions or through the removal of hydrophobic regions of the drug from contact with water.

Keeping the above points in mind, the binding event of each of the five *Vinca* alkaloids to β-tubulin will likely be a fast, simple event that is driven by non-covalent interactions. This agrees with the previously proposed mechanism of rapid and reversible binding [9]. The present study did not find any reasons for the binding of VFL to the *Vinca* domain to be considerably different than the other four *Vinca* alkaloids studied, as was found by Kruczynski [13]. However, this is not to say that more in-depth simulations or calculations would not discover such reasons – this study is only a model of a single bound state and does not model the binding dynamics of the *Vinca* alkaloids.

5.4. Validity of model

The 1Z2B crystal structure is the only set of high-resolution coordinates of a *Vinca* alkaloid bound to tubulin known to date. To the best of the authors' knowledge, the present paper reports the first comprehensive MD simulation of all five *Vinca* alkaloids

[4] Found to be residues β173–β 211 in [10] and β172–β177, β208–β 225 in [40].

bound to tubulin based on the 1Z2B crystal structure (VLB was the only *Vinca* alkaloid recently studied [26]). The binding domain and mode in this structure agree well with other studies on the binding of the *Vinca* alkaloids. The calculations and simulations on the free *Vinca* alkaloids demonstrate that only one conformation for each will be present in any significant quantity at 310 K. As this equilibrium conformation closely resembles the conformation found for VLB in 1Z2B, the binding mode in 1Z2B must be considered highly likely for all the *Vinca* alkaloids studied. Furthermore, in the MD simulations of the *Vinca* alkaloids bound to tubulin, the complexes do not destabilize in any apparent way or expel the *Vinca* alkaloid from the binding domain, indicating at least basic stability.

6. Conclusions

The *Vinca* alkaloids studied here have been demonstrated to have one preferred equilibrium and minimum energy conformation with main dihedral angle near 200°. It is highly likely that this conformation is prerequisite to a *Vinca* alkaloid congener to function as an anti-mitotic agent. Modifications to the drug in rational drug design that disrupt this equilibrium conformation may destroy the activity of the drug. Similarly, modifications that work within and strengthen this preferred conformation may have a better chance of efficacy. The structural feature that gives rise to this preferred conformation is the sterically induced distortion of the upper portion of the *Vinca* alkaloids. The unique equilibrium angles found in VNO and VFL are likely due to the modifications made to the upper portions of those drugs. Therefore, the upper portion backbone of the *Vinca* alkaloids is of particular importance as changes may seriously affect the affinity for tubulin and hence the activity of a *Vinca* alkaloid drug.

Acknowledgements

The authors wish to thank Dr. Mary Ann Jordan for insightful comments regarding the experimental determination of the VLB binding sites on microtubules. The present work was supported by several agencies. EK thanks the Alberta Ingenuity Fund, the Mathematics of Information Technology and Complex Systems (MITACS), and the Natural Sciences and Engineering Research Council of Canada (NSERC) for graduate scholarships and internships. MK thanks NSERC for continuing support of his research. JT thanks NSERC, the Alberta Cancer Foundation, the Allard Foundation, and the Alberta Advanced Education and Technology for research support. Results presented in this work were obtained on several computer installations, funded in part by NSERC Discovery and Research Grants to MK. The authors are grateful to the anonymous Reviewers whose comments and questions improved the present paper.

References

[1] R. Bau, K.K. Jin, Crystal structure of vinblastine, Journal of the Chemical Society-Perkin Transactions 1 (13) (2000) 2079–2082.
[2] B. Gigant, C.G. Wang, R.B.G. Ravelli, F. Roussi, M.O. Steinmetz, P.A. Curmi, A. Sobel, M. Knossow, Structural basis for the regulation of tubulin by vinblastine, Nature 435 (2005) 519–522.
[3] J. Duffin, Poisoning the spindle: serendipity and discovery of the anti-tumour properties of the vinca alkaloids, Canadian Bulletin of Medical History 17 (2000) 155–192.
[4] M.J. Sweeney, G.B. Boder, G.J. Cullinan, H.W. Culp, W.D. Daniels, R.W. Dyke, K. Gerzon, R.E. Mcmahon, R.L. Nelson, G.A. Poore, G.C. Todd, Anti-tumor activity of deacetyl vinblastine amide sulfate (vindesine) in rodents and mitotic accumulation studies in culture, Cancer Research 38 (9) (1978) 2886–2891.
[5] N. Langlois, F. Gueritte, Y. Langlois, P. Potier, Application of a modification of Polonovski reaction to synthesis of vinblastine-type alkaloids, Journal of the American Chemical Society 98 (22) (1976) 7017–7024.
[6] P. Mangeney, R.Z. Andriamialisoa, J.Y. Lallemand, N. Langlois, Y. Langlois, P. Potier, 5′-nor anhydrovinblastine – prototype of a new class of vinblastine derivatives, Tetrahedron 35 (18) (1979) 2175–2179.
[7] B.T. Hill, Vinflunine, a second generation novel vinca alkaloid with a distinctive pharmacological profile, now in clinical development and prospects for future mitotic blockers, Current Pharmaceutical Design 7 (13) (2001) 1199–1212.
[8] M.A. Jordan, L. Wilson, Microtubules as a target for anticancer drugs, Nature Reviews Cancer 4 (4) (2004) 253–265.
[9] M.A. Jordan, L. Wilson, Kinetic-analysis of tubulin exchange at microtubule ends at low vinblastine concentrations, Biochemistry 29 (11) (1990) 2730–2739.
[10] S.S. Rai, J. Wolff, Localization of the vinblastine-binding site on beta-tubulin, Journal of Biological Chemistry 271 (25) (1996) 14707–14711.
[11] S.K. Chatterjee, J. Laffray, P. Patel, R. Ravindra, Y. Qin, M.E. Kuehne, S.L. Bane, Interaction of tubulin with a new fluorescent analogue of vinblastine, Biochemistry 41 (47) (2002) 14010–14018.
[12] A. Mitra, D. Sept, Localization of the antimitotic peptide and depsipeptide binding site on beta-tubulin, Biochemistry 43 (44) (2004) 13955–13962.
[13] A. Kruczynski, J.M. Barret, C. Etievant, F. Colpaert, J. Fahy, B.T. Hill, Antimitotic and tubulin-interacting properties of vinflunine, a novel fluorinated vinca alkaloid, Biochemical Pharmacology 55 (5) (1998) 635–648.
[14] E.K. Rowinsky, A.W. Tolcher, Chemotherapy Source Book, 3rd ed., Lippincott Williams and Wilkins, 2001 (Chapter 23).
[15] J. Lowe, H. Li, K.H. Downing, E. Nogales, Refined structure of alpha beta-tubulin at 3.5 Å resolution, Journal of Molecular Biology 313 (5) (2001) 1045–1057.
[16] W. Humphrey, A. Dalke, K. Schulten, VMD – visual molecular dynamics, Journal of Molecular Graphics 14 (1) (1996) 33–38.
[17] J.W. Moncrief, W.N. Lipscomb, Structures of leurocristine (vincristine) and vincaleukoblastine. X-ray analysis of leurocristine methiodide, Journal of the American Chemical Society 87 (21) (1965) 4963–4964.
[18] B.K. Hunter, L. Dhall, J.K.M. Sanders, The conformation of vinblastine in solution as determined by NOE difference spectroscopy, Journal of the Chemical Society-Perkin Transactions 1 (3) (1983) 657–665.
[19] E. Gaggelli, G. Valensin, N.J. Stolowich, H.J. Williams, A.I. Scott, Conformation of vinblastine in aqueous-solution determined by 2d H-1-NMR and C-13-NMR spectroscopy, Journal of Natural Products 55 (3) (1992) 285–293.
[20] N.L. Allinger, Conformational analysis. 130. MM2 – hydrocarbon force-field utilizing V1 and V2 torsional terms, Journal of the American Chemical Society 99 (25) (1977) 8127–8134.
[21] C.W. Andrews, J. Wisowaty, A.O. Davis, R.C. Crouch, G.E. Martin, Molecular modeling, NMR-spectroscopy, and conformational-analysis of 3′, 4′-anhydrovinblastine, Journal of Heterocyclic Chemistry 32 (3) (1995) 1011–1017.
[22] F. Mohamadi, N.G.J. Richards, W.C. Guida, R. Liskamp, M. Lipton, C. Caufield, G. Chang, T. Hendrickson, W.C. Still, Macromodel – an integrated software system for modeling organic and bioorganic molecules using molecular mechanics, Journal of Computational Chemistry 11 (4) (1990) 440–467.
[23] N.L. Allinger, Y.H. Yuh, J.H. Lii, Molecular mechanics – the MM3 force-field for hydrocarbons. 1, Journal of the American Chemical Society 111 (23) (1989) 8551–8566.
[24] J.H. Lii, N.L. Allinger, Molecular mechanics – the MM3 force-field for hydrocarbons. 2. Vibrational frequencies and thermodynamics, Journal of the American Chemical Society 111 (23) (1989) 8566–8575.
[25] J.H. Lii, N.L. Allinger, Molecular mechanics – the MM3 force-field for hydrocarbons. 3. The van der Waals potentials and crystal data for aliphatic and aromatic hydrocarbons, Journal of the American Chemical Society 111 (23) (1989) 8576–8582.
[26] S. Rendine, S. Pieraccini, M. Sironi, Vinblastine perturbation of tubulin protofilament structure: a computational insight, Physical Chemistry Chemical Physics 12 (2010) 15530–15536.
[27] D.A. Case, T.A. Darden, T.E. Cheatham III, C.L. Simmerling, J. Wang, R.E. Duke, R. Luo, K.M. Merz, D.A. Pearlman, M. Crowley, R.C. Walker, W. Zhang, B. Wang, S. Hayik, A. Roitberg, G. Seabra, K.F. Wong, F. Paesani, X. Wu, S. Brozell, V. Tsui, H. Gohlke, L. Yang, C. Tan, J. Mongan, V. Hornak, G. Cui, P. Beroza, D.H. Mathews, C. Schafmeister, W.S. Ross, P.A. Kollman, Amber 9, University of California, San Francisco, 2006.
[28] I. Massova, P.A. Kollman, Computational alanine scanning to probe protein–protein interactions: a novel approach to evaluate binding free energies, Journal of the American Chemical Society 121 (1999) 8133–8143.
[29] L. Wilson, M.A. Jordan, A. Morse, R.L. Margolis, Interaction of vinblastine with steady-state microtubules in vitro, Journal of Molecular Biology 159 (1) (1982) 125–149.
[30] M.A. Jordan, R.L. Margolis, R.H. Himes, L. Wilson, Identification of a distinct class of vinblastine binding sites on microtubules, Journal of Molecular Biology 187 (1) (1986) 61–73.
[31] R.J. Toso, M.A. Jordan, K.W. Farrell, B. Matsumoto, L. Wilson, Kinetic stabilization of microtubule dynamic instability invitro by vinblastine, Biochemistry 32 (5) (1993) 1285–1293.
[32] H.-W. Wang, E. Nogales, Nucleotide-dependent bending flexibility of tubulin regulates microtubule assembly, Nature 435 (2005) 911–915.
[33] D. Panda, M.A. Jordan, K.C. Chu, L. Wilson, Differential effects of vinblastine on polymerization and dynamics at opposite microtubule ends, The Journal of Biological Chemistry 271 (1996) 29807–29812.
[34] E. Nogales, S.G. Wolf, I.A. Khan, R.F. Luduena, K.H. Downing, Structure of tubulin at 6.5 Å and location of the taxol-binding site, Nature 375 (1995) 424–427.
[35] H. Li, D.J. DeRosier, W.V. Nicholson, E. Nogales, K.H. Downing, Microtubule structure at 8 Å resolution, Structure 10 (10) (2002) 1317–1328.
[36] E. Nogales, S.G. Wolf, K.H. Downing, Structure of the αβ tubulin dimer by electron crystallography, Nature 391 (1998) 199–203.

[37] J.H. Nettles, H. Li, B. Cornett, J.M. Krahn, J.P. Snyder, K.H. Downing, The binding mode of epothilone A on α, β-tubulin by electron crystallography, Science 305 (5685) (2004) 866–869.
[38] B. Gigant, P.A. Curmi, C. Martin-Barbey, E. Charbaut, S. Lachkar, L. Lebeau, S. Siavoshian, A. Sobel, M. Knossow, The 4 Å X-ray structure of a tubulin:stathmin-like domain complex, Cell 102 (6) (2000) 809–816.
[39] R.B. Ravelli, B. Gigant, P.A. Curmi, I. Jourdain, S. Lachkar, A. Sobel, M. Knossow, Insight into tubulin regulation from a complex with colchicine and a stathmin-like domain, Nature 428 (2004) 198–202.
[40] J.T. Huzil, R.F. Luduena, J. Tuszynski, Comparative modelling of human beta tubulin isotypes and implications for drug binding, Nanotechnology 17 (4) (2006) S90–S100.
[41] J.T. Huzil, K. Chen, L. Kurgan, J.A. Tuszynski, The roles of beta-tubulin mutations and isotype expression in acquired drug resistance, Cancer Informatics 3 (2007) 159–181.
[42] R. Bai, N.A. Durso, D.L. Sackett, E. Hamel, Interactions of the sponge-derived antimitotic tripeptide hemiasterlin with tubulin: comparison with dolastatin 10 and cryptophycin 1, Biochemistry 38 (43) (1999) 14302–14310.
[43] Spartan, Spartan '04 for Macintosh, Wavefunction Inc., Irvine, CA, 2004.
[44] T.A. Halgren, Merck molecular force field. 1. Basis, form, scope, parameterization, and performance of MMFF94, Journal of Computational Chemistry 17 (5–6) (1996) 490–519.
[45] T.A. Halgren, Merck molecular force field. 2. MMFF94 van der Waals and electrostatic parameters for intermolecular interactions, Journal of Computational Chemistry 17 (5–6) (1996) 520–552.
[46] T.A. Halgren, Merck molecular force field. 3. Molecular geometries and vibrational frequencies for MMFF94, Journal of Computational Chemistry 17 (5–6) (1996) 553–586.
[47] T.A. Halgren, R.B. Nachbar, Merck molecular force field. 4. Conformational energies and geometries for MMFF94, Journal of Computational Chemistry 17 (5–6) (1996) 587–615.
[48] T.A. Halgren, Merck molecular force field. 5. Extension of MMFF94 using experimental data, additional computational data, and empirical rules, Journal of Computational Chemistry 17 (5–6) (1996) 616–641.
[49] A.A. Granovsky, PC-GAMESS version 7.0 [online], 2005.
[50] M.W. Schmidt, K.K. Baldridge, J.A. Boatz, S.T. Elbert, M.S. Gordon, J.H. Jensen, S. Koseki, N. Matsunaga, K.A. Nguyen, S. Su, T.L. Windus, M. Dupuis, J.J.A. Montgomery, General atomic and molecular electronic structure system, Journal of Computational Chemistry 14 (1993) 1347–1363.
[51] J.D. Head, M.C. Zerner, A Broyden-Fletcher-Goldfarb-Shanno optimization procedure for molecular geometries, Chemical Physics Letters 122 (3) (1985) 264–270.
[52] A. Banerjee, N. Adams, J. Simons, R. Shepard, Search for stationary-points on surface, Journal of Physical Chemistry 89 (1) (1985) 52–57.
[53] K. Nam, J.L. Gao, D.M. York, An efficient linear-scaling Ewald method for long-range electrostatic interactions in combined QM/MM calculations, Journal of Chemical Theory and Computation 1 (1) (2005) 2–13.
[54] J.P. Ryckaert, G. Ciccotti, H.J.C. Berendsen, Numerical-integration of Cartesian equations of motion of a system with constraints – molecular-dynamics of *n*-alkanes, Journal of Computational Physics 23 (3) (1977) 327–341.
[55] J.M. Wang, R.M. Wolf, J.W. Caldwell, P.A. Kollman, D.A. Case, Development and testing of a general Amber force field, Journal of Computational Chemistry 25 (9) (2004) 1157–1174.
[56] H. Flyvbjerg, H.G. Petersen, Error-estimates on averages of correlated data, Journal of Chemical Physics 91 (1) (1989) 461–466.
[57] Y. Duan, C. Wu, S. Chowdhury, M.C. Lee, G.M. Xiong, W. Zhang, R. Yang, P. Cieplak, R. Luo, T. Lee, J. Caldwell, J.M. Wang, P. Kollman, A point-charge force field for molecular mechanics simulations of proteins based on condensed-phase quantum mechanical calculations, Journal of Computational Chemistry 24 (16) (2003) 1999–2012.
[58] K.L. Meagher, L.T. Redman, H.A. Carlson, Development of polyphosphate parameters for use with the AMBER force field, Journal of Computational Chemistry 24 (9) (2003) 1016–1025.
[59] P. Magnus, M. Ladlow, J. Elliott, Models for a hypothetical mechanism of action of the anticancer agent vinblastine, Journal of the American Chemical Society 109 (25) (1987) 7929–7930.
[60] L. He, C.-P.H. Yang, S. Horwitz, Mutations in beta-tubulin map to domains involved in regulation of microtubule stability in epothilone-resistant cell lines, Molecular Cancer Therapeutics 1 (2001) 3–10.
[61] M. Hari, Y. Wang, S. Veeraraghavan, F. Cabral, Mutations in alpha- and beta-tubulin that stabilize microtubules and confer resistance to colcemid and vinblastine, Molecular Cancer Therapeutics 2 (2003) 597–605.
[62] M.E. Kuehne, W.G. Bornmann, I. Marko, Y. Qin, K.L. LeBoulluec, D.A. Frasier, F. Xu, T. Mulamba, C.L. Ensinger, L.S. Borman, A.E. Huot, C. Exon, F.T. Bizzarro, J.B. Cheung, S.L. Bane, Syntheses and biological evaluation of vinblastine congeners, Organic and Biomolecular Chemistry 1 (12) (2003) 2120–2136.